JOURNAL OF MATERIALS SCIENCE 27 (1992) 1202–1206

Microstructural observations of two deformed partially stabilized zirconia ceramics using acoustic microscopy

A. F. FAGAN, G. A. D. BRIGGS, J. T. CZERNUSZKA, C. B. SCRUBY*
Department of Materials, University of Oxford, Parks Road, Oxford, OX1 3PH, UK,

Ceramics containing zirconia exhibit increased fracture toughness because of the transformation mechanism. Because the acoustic microscope yields contrast at regions of differing elastic properties, it is possible to obtain unique information from these regions. Acoustic micrographs of phase-transformed regions surrounding Vickers indentations showed contrast within grains. Radial cracks were strongly visible, while up to five types of line contrast have been imaged. Much of the contrast in the acoustic micrographs is interpreted in terms of the interaction between Rayleigh waves and the microstructure of the zirconia ceramic. Line-contrast types A and B are accounted for in the literature while types C–E are new.

1. Introduction

Toughening in partially stabilized zirconias (PSZs) and ceramics containing zirconia is dependent on the tetragonal (t) to monoclinic (m) phase transformation which occurs in constrained metastable composites [1, 2]. In this paper a method that is sensitive to the microstructural phases in zirconia ceramics is presented. Scanning acoustic microscopy (SAM) uses a water-coupled lens to transmit a focused beam of high-frequency sound on to the specimen [3]. Contrast is produced from acoustic energy reflected by the surface after first interacting with it to a depth of approximately one Rayleigh wavelength (λ_R). In acoustic microscopy it is possible to obtain images from regions of polymorphic zirconia because contrast is produced by areas of differing elastic properties [4].

The stress-induced phase transformation exhibited by zirconia materials can be initiated by indenting a sample of PSZ [5] which is then examined after carefully polishing the surface to make it flat without introducing residual stresses [6, 7]. The distribution of monoclinic material in the acoustic micrographs can be verified by cathodo-luminescence (CL) because the monoclinic polymorph produced during indentation is strongly luminescent [5].

2. Experimental procedure

The ceramics investigated were sub-eutectoid aged ZrO_2–2 wt %MgO (MPSZ) and as-fired ZrO_2–4 wt % CaO(CPSZ). Standard metallographic preparation of the specimens involved mounting in cold-cured epoxy and lapping using cast iron or tin laps with diamond powders of 6 and 1 μm. Vickers indentations were introduced into the lapped surfaces using loads of 10 kg. Final polishing using 0.25 μm diamond paste removed any plastically deformed material which had been vertically displaced during indentation.

Parallel studies of the indentations were carried out with the Camscan SEM (CL mode), polarized reflected light microscopy (PRLM) and an Ernst Leitz scanning acoustic microscope (Elsam). The Elsam lens had an operating frequency range of 1.3–2 GHz with half-angle, $\alpha = 50°$ and cavity radius, $r = 40°$. For the MPSZ, the Elsam was used at a frequency of 1.3 GHz giving a wavelength in the couplant water, λ_W, of 1.15 μm and a Rayleigh wavelength, λ_R, in the ceramic of 2.44 μm. Micrographs for the CPSZ were obtained at frequencies of 1.3 and 2 GHz giving respective values for λ_R of 2.55 and 1.66 μm. The considerable variation in λ_R at a given frequency may be attributable to chemical variations between the two PSZs, but zirconia has an especially high anisotropy [4]. Rayleigh wave velocities, V_R, of the two ceramics were obtained by line-focus-beam microscopy (LFBM), using a Kushibiki line-focus lens with a frequency range of 150–300 MHz and respective α and r values of 60° and 1 mm. Rayleigh wave velocities of 3175 m s^{-1} for MPSZ and 3317 m s^{-1} for CPSZ were obtained using Kushibiki and Chubachi's technique of $V(z)$ analysis [8]. After acoustic microscopy the PSZ samples were sputter-coated with gold to 10 nm before placing them in the SEM. The "Camscan" was adapted for CL by covering the secondary electron detector and using an "S"-shaped polymethylmethacrylate (PMMA) light-guide of 17 mm diameter attached to a photo-multiplier. The light guide was placed with its free end facing the specimen at a

*also AEA Technology, Harwell, Oxon, OX11 0RA, UK

0022–2461

working distance of 40 mm. Imaging and location of the specimen inside the SEM sample chamber was achieved using a Robinson scintillation type backscatter electron (BSE) detector. Typical working conditions were: electron energy 20 keV, specimen current $7–8 \times 10^{-8}$ A, working distance 20 mm. Images were obtained without specimen tilt.

3. Results

In the acoustic micrographs of Figs 1, 3, 5 and 6, grain boundaries, intra-grain regions, a deformed region around the indentation, and cracks may be seen. Comparative CL and PRLM micrographs of the areas shown by Elsam appear for the MPSZ in Figs 2 and 4 and for the CPSZ in Figs 7 and 8. Elsam micrographs

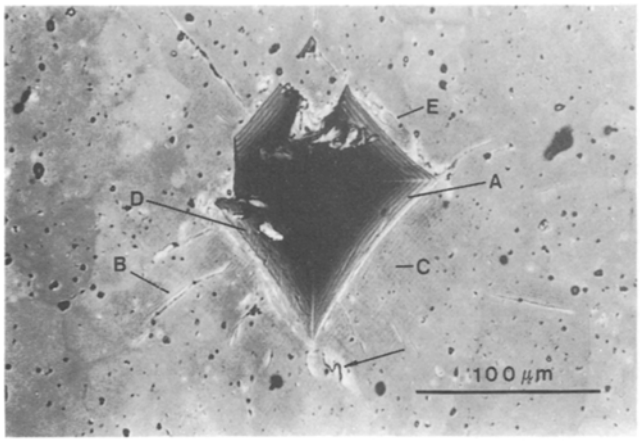

Figure 1 Elsam, 1.3 GHz, $z = -1$ μm. MPSZ grains and line contrast types A–E (corresponding to types I–V [6]).

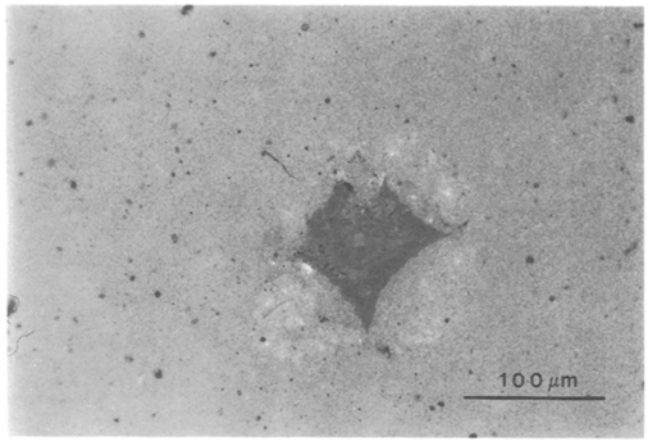

Figure 4 PRLM. Indented MPSZ. The same region as the Elsam picture in Fig. 1.

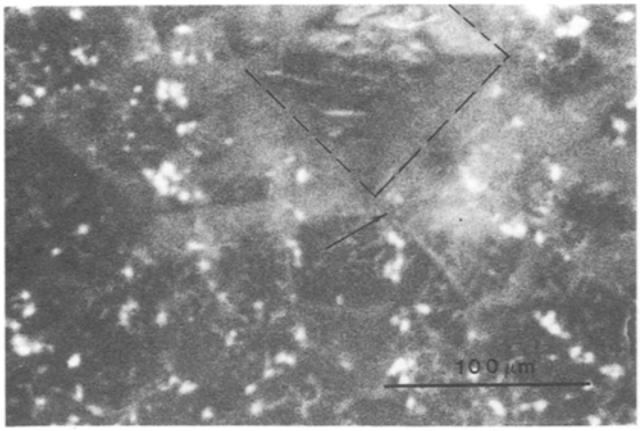

Figure 2 SEM/CL lower three-quarters view of the MPSZ indentation in Fig. 1.

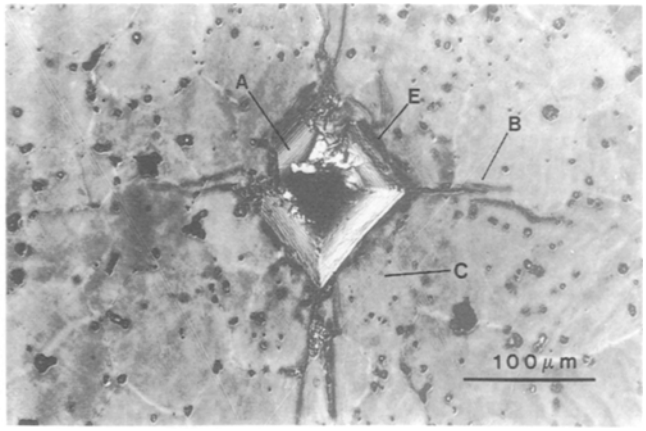

Figure 5 Elsam, 1.3 GHz, $z = -4$ μm. CPSZ, line-contrast and grains.

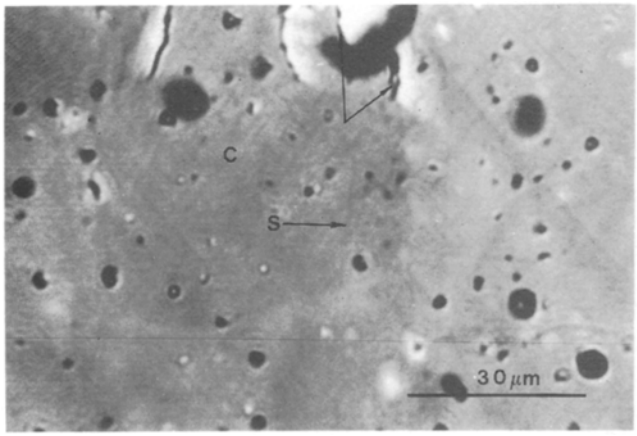

Figure 3 Elsam, 1.3 GHz, $z = -1$ μm. MPSZ type C lines. The arrowed upper crack is that shown arrowed in Fig. 1.

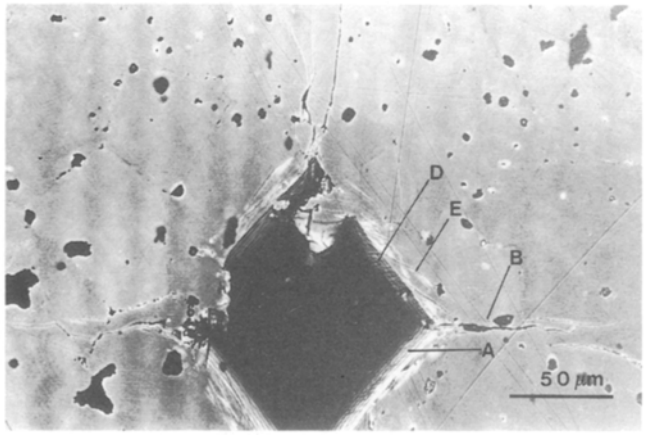

Figure 6 Elsam, 2.0 GHz, $z = -0.6$ μm. CPSZ, without type C line contrast.

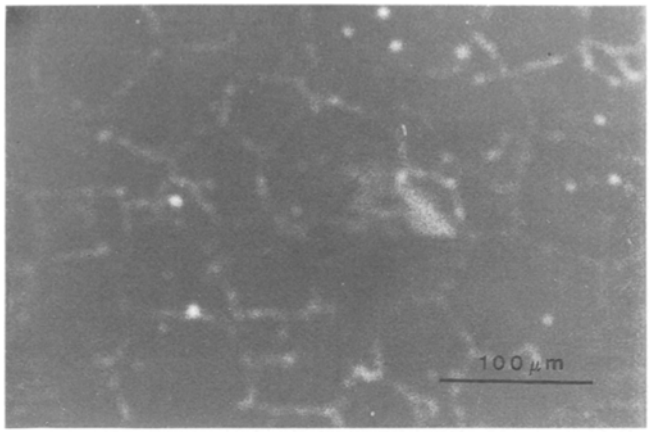

Figure 7 SEM/CL, of the area shown by Elsam in Fig. 5. The bright network at the grain boundary is caused by m-phase zirconia.

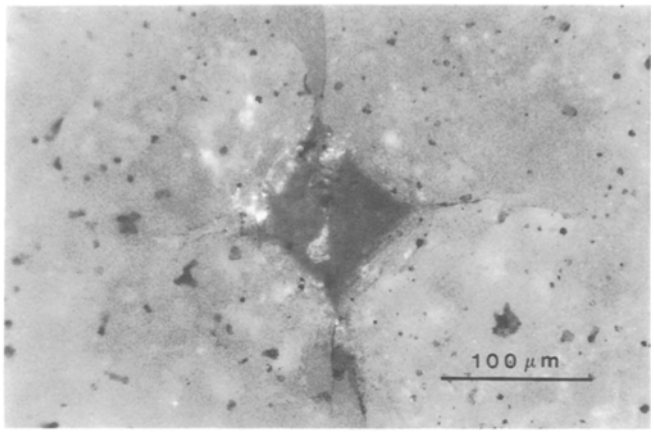

Figure 8 PRLM of the region shown by Elsam in Fig. 5.

TABLE I Fringe contrast from acoustic micrographs of PSZ materials

Type	Location	Appearance	Spacing	Comments
A	Inside the indentation of flat samples	Concentric rings	$\lambda_W/2$	May show height variations
B	Cracks/grain boundaries	Straight or bent	$\lambda_R/2$	Also occurs as L wave fringes
C	Flat surface near indent	Cross-hatched two sets of parallel lines	2.3 μm	Occurs at $\leqslant$ 70 μm from indent
D	Slopes of indentation	Intersected by type A	$\geqslant$ 2.3 μm	May meet type C or D
E	Flat surface of CPSZ specimen	Thin curved	Variable $\leqslant$ 8 μm	

in Figs 1, 5 and 6 show the association of the different line types with the indentation.

Acoustic microscopy gives rise to strong microstructural contrast and in many instances the contrast correlates with that from PRLM and CL. Fringes A–B correspond to those previously called types I–V [6]. Acoustic fringes or line types A (water-ripple) and B (Yamanaka-ripple) are generated by many materials. In Figs 1, 5 and 6, type A fringes of height $\lambda_W/2$ occur as topographical contours on the surfaces of the MPSZ and the CPSZ. Type B fringes are generated by the reflection of Rayleigh (or bulk) waves from elastic discontinuities such as grain boundaries and cracks [9]. The spacing of type B fringes is a function of the imaging frequency and the Rayleigh wave velocity, V_R, in the PSZ. MPSZ has a $V_R = 3175\ m\,s^{-1}$ which at 1.3 GHz gives a single-fringe spacing, $\lambda_R/2 = 1.22$ μm. CPSZ has $V_R = 3317\ m\,s^{-1}$ and is imaged at both 1.3 and 2 GHz giving respective values for $\lambda_R/2$ of 1.28 and 0.83 μm. Fringe types A and B are found in acoustic micrographs of many materials but line types C–E have been seen for PSZs only. Type C contrast in Figs 1, 3 and 5 occurs as two sets of interlocking parallel lines which are 2.3 μm apart. For CPSZ and MPSZ the type C lines occur in an area 60–100 μm from the indentation. Parallel type D lines occur for the MPSZ in Fig. 1 and for the CPSZ in Fig. 6. Type D lines cross type A fringes at acute angles. It can be inferred from Fig. 1 that the spacing of type D lines is based on that of the type C fringe value of 2.3 μm because some of the MPSZ type C and D lines meet at the edge of the indentation. Irregularly shaped type E fringes appear at 1.3 GHz for the MPSZ and the CPSZ in Figs 1 and 5, respectively, and at 2 GHz for the CPSZ in Fig. 6. Type E lines are located close to the edge of the indentations in Figs 1, 5 and 6. The acoustic line morphologies encountered in the PSZ results section are listed in Table I.

4. Discussion

4.1. Type A line contrast

Type A lines form contours which are shown inside the indentation of Figs 1, 5 and 6. Type A fringes shown are, in some instances, accompanied by other regions of similar contrast. Because the additional contrast in the type A area appears to be less regular and discontinuous, it is unlikely that water-ripple is solely responsible for its formation. Perhaps type A fringes are not entirely the result of topographic changes but are, instead, partly caused by fine cracks which are approximately parallel to the respective edges of the indentation. The fine cracked structure in the type A region of the indentation is probably

caused by the shearing mechanism which accompanies indentation of the PSZs.

4.2. Type B fringes

Type B fringes appear in negatively defocused images because under these conditions Rayleigh wave imaging is enhanced. Examples of type B or Rayleigh fringes occur in all of the defocused Elsam micrographs. The theoretical spacing of Rayleigh fringes is given by λ_R where $\lambda_R = V_R/f$ and f is the operating frequency. V_R is obtained from analysis of respective $V(z)$s for MPSZ and CPSZ. Values for V_R measured by Kushibiki's method are: for MPSZ, 3175 m s^{-1}, and for CPSZ, 3317 m s^{-1}. Using calculated values of V_R, the respective type B fringes are separated by 2.44 and 2.55 μm for MPSZ and CPSZ. The calculated type B spacings are close to the measured values of 2.3 μm from the type B fringes in Figs 1 and 5 for MPSZ and CPSZ, respectively. Up to six type B fringes surround the cracks and pores of the MPSZ in Figs 1 and 3 and the CPSZ in Figs 5 and 6.

4.3. Type C line contrast

The 1.3 GHz type C lines, shown respectively for MPSZ and CPSZ in Figs 1 and 5, occupy larger areas than type B fringes. That part of the cross-hatched type C line which is parallel to the edge of the indentation forms more than 20 lines. They are most evident in grains of the MPSZ touching the lower edges of the indentation. This is the same region occupied by the bright lobes in the CL and the PRLM images shown in Figs 2 and 4. Similarly, the Elsam image of CPSZ in Fig. 5, type C lines are associated with the lower area of the indentation and with the bright lobes of the respective PRLM image in Fig. 8. However, the CL image of CPSZ in Fig. 7 does not share with the CL micrograph of MPSZ the same bright lobal contrast at the indentation, instead, the indentation is associated with a region of subdued or dark contrast. Regions of bright contrast in the CPSZ CL picture are associated with one face of the indentation, but mostly with the grain-boundary regions. Contrast in PRLM images is caused by interaction of the incident and reflected polarized rays from sub-surface cracks. SAM type C regions of CPSZ and MPSZ extend further from the indentation than do the corresponding bright lobes in the PRLM micrographs.

Some of the Elsam type C regions are occupied by the remains of scratches from polishing; these are shown by the MPSZ in Fig. 3 and by the CPSZ in Figs 5 and 6. Neither of the PSZs shows evidence that scratching is a precursor in the development of the type C lines because the scratches are randomly oriented with respect to the two main axes of the type C contrast. Micrographs supporting this are: Fig. 3, for MPSZ and Figs 5 and 6 for the CPSZ. Fig. 3 shows scratches, one of them marked "S", which traverse the type C contrast from the area under the lowest apex of the indentation.

4.4. Types D and E line contrast

Type D lines occur on both of the PSZs while type E lines are best resolved in Fig. 6 where they occur as fine cracks outside the indentation in a fracture zone of width 20 μm. Type D lines appear to recede into the indentation whereas type E lines occupy the top surface of the CPSZ specimen in Fig. 6. Type E lines are irregularly shaped with a spacing of approximately 8 μm. Type D and type E lines meet at the edges of the indentation where they have the appearance of fine cracks.

4.5. Comparison of contrast from acoustic and CL micrographs

In the SAM micrographs of Figs 1, 3, 5 and 6 the largest effects on bulk material contrast are the result of intergranular changes in orientation of the crystal elastic tensors and, to a lesser extent, on the local modulus changes in regions of the tetragonal to monoclinic phase change associated with the indentation. More localized contrast is the result of Rayleigh wave interaction with elastic discontinuities such as cracks, pores and grain boundaries. There may be other contrast in the acoustic micrographs which can be related to contrast in the CL images, because factors affecting luminescent behaviour in PSZs may cause changes in the propagating leaky Rayleigh wave. Possible causes of CL behaviour in PSZs which may also affect the Rayleigh wave are: the intrinsic band structure of certain materials [10]; localized effects such as electron states near impurities [11]; lattice defects and stress fields [12]. However, the lattice defects in PSZs which may cause CL have widths of the order of the unit cell dimensions. Consequently, lattice defects are unresolvable when using SAM under normal conditions at frequencies $\leqslant 2$ GHz and $\lambda_W = 0.75$ μm. If an aggregate of lattice defects is examined by SAM and its size exceeds λ_W, then the aggregate can be resolved. Contrast from impurities might arise from modulus variations and associated local changes of acoustic impedance. Enhanced contrast through Rayleigh wave scattering occurs where marked elastic changes exist between impurity particles and the matrix or at the interface dividing them.

5. Conclusions

The SAM offers a technique for the micro-analysis of PSZ materials with 1 μm resolution at 1.3 GHz and 0.75 μm resolution at 2 GHz. Enhancement of contrast through Rayleigh wave and impedance imaging has allowed phase discrimination of what is assumed to be tetragonal and monoclinic materials in the CPSZ and MPSZ. Phase-transformed materials are associated with shear banding in high-stress regions surrounding indentations. In addition to the Rayleigh fringes and water-ripple fringes, three additional types of contrast were identified in the SAM micrographs of the PSZs. The additional fringes, referred to as types C–E, may have a microstructural basis and occupy regions where the tetragonal to monoclinic phase

change has occurred. Further work is recommended to identify the phases in the shear-band region and to confirm line-types C, D and E.

By applying SAM with CL, and PRLM it has been possible to suggest a microstructural basis for contrast derived from the CPSZ and MPSZ ceramics. Our conclusions are as follows.

1. Type A fringes may be a combination of topographic fringes caused by water-ripple and sheared regions of transformed material which occur parallel to the surface.

2. Type B fringes are Rayleigh wave reflections. Fringe separation is 2.3 μm.

3. Cross-hatched type C lines with spacing 2.3 μm may be the result of interference between propagating Rayleigh waves as a result of scattering from shear bands.

4. Type D lines, detected on the indentation faces, may indicate the depth of the transformed region. Some type D lines meet type C and E lines at the edge of the indentation.

5. Type E lines are perhaps cracks associated with the deformed region. They are located near to the edge of the indentation.

6. Scratches on the surface of PSZs do not relate to the type C lines.

7. Grain boundaries of the MPSZ are shown by SAM only while grains in the CPSZ are shown by CL and SAM.

8. CPSZ and MPSZ grains show anisotropic contrast in the SAM micrographs.

Acknowledgements

We thank the following people and institutions for providing equipment and support: Dr J. Kushibiki, Tohoku University, Sendai, Japan, for the line focus beam acoustic microscope; Wild Leitz GmbH, Wetzlar, Germany, for the Elsam scanning acoustic microscope; the National Physical Laboratory (NPL) for use of the Camscan; Dr D. S. Spencer, Agricultural Food Research Council (AFRC), Sileso, Bedfordshire, for help with $V(z)$ acquisition and analysis; Dr M. V. Swain, CSIRO, Melbourne for PSZ materials. Andrew Fagan also thanks the SERC for providing a CASE award, NPL who were his industrial sponsors, and the present and late members of the DMM group at NPL for their good-humoured assistance.

References

1. R. GARVIE, R. HANNINK and R. PASCOE, *Nature* **258** (1975) 703.
2. A. EVANS and A. HEUER, *J. Amer. Ceram. Soc.* **63** (1980) 241.
3. G. A. D. BRIGGS, in "An Introduction to Scanning Acoustic Microscopy" Royal Microscopy Society. Microscopy Handbook 12 (Oxford University Press, Oxford, 1985).
4. *Idem.*, "Acoustic Microscopy" (Oxford University Press, Oxford, 1991).
5. J. T. CZERNUSZKA and T. PAGE, *J. Amer. Ceram. Soc.* **68** (1985) 196.
6. A. F. FAGAN, G. A. D. BRIGGS, J. T. CZERNUSZKA and C. B. SCRUBY, *Trans. R. Microsc. Soc.* (1990) 81.
7. A. F. FAGAN, DPhil, University of Oxford (1990) Ch. 3.
8. J. KUSHIBIKI and N. CHUBACHI, *IEEE Trans. Sonics Ultrasonics* **SU-32** (1985) 189.
9. K. YAMANAKA and Y. ENOMOTO, *J. Appl. Phys.* **52** (1982) 846.
10. W. STRECHLOW and E. COOK, *Phys. Chem. Ref. Data* **2** (1973) 163.
11. M. MUIR and P. GRANT, in "Quantitative Scanning Electron Microscopy" (New York, Academic Press, New York, 1974).
12. S. PENNYCOOK, L. BROWN and A. CRAVEN, *Phil. Mag.* **A41** (1980) 589.

Received 7 November 1990
and accepted 4 April 1991